Cryo-TEMPO

Algorithm Theoretical Basis Document

Coastal Ocean

Prepared by	:	F. Nencioli	22/6/2021
Checked by	:	S. Hendricks	20/7/2021
Approved by	:		

Change Log

Issue	Author	Affected Section	Change	Status
0	F. Nencioli	All	Document Creation	Complete
1.1	F. Nencioli	All	Version 1 Content	Complete
1.2	F. Nencioli	All	Version 1 Revisions	Complete
2.1	F. Nencioli	All	Version 2 Revisions	In Review

Acronyms and Abbreviations

AD	Applicable Document
ADT	Absolute Dynamic Topography
CLS	Collecte Localisation Satellites
CNES	Centre National des Etudes Spatiales (French Space Agency)
COP	CryoSat Ocean Processor
DAC	Dynamic Atmospheric Correction
DTU	Technical University of Denmark
DUACS	Data Unification and Altimeter Combination System
ECMWF	European Centre for Medium-Range Weather Forecasts
ESA	European Space Agency
FES	Finite Element Solution
GIM	Global Ionosphere Maps
GNSS	Global Navigation Satellite Systems
GOP	Geophysical Ocean Product
GPD+	GNSS derived Path Delay Plus
GSHHG	Global Self-consistent, Hierarchical, High-resolution Geography
HFA	High Frequency adjustment
JPL	Jet Propulsion Laboratory
LRM	Low Resolution Mode
LUT	Look-up table
MDT	Mean Dynamic Typography
MLE	Maximum Likelihood Estimation
MLE4	Altimeter waveform MLE retracker with 4 free parameters that are estimated (Range, significant wave height, radar backscatter, and altimeter attitude)
MOG2D	Modèle 2D d'Ondes de Gravité, a barotropic oceanic model
MSS	Mean Sea Surface
SAMOSA	SAR Altimetry MOde Studies and Applications
SAMOSA2	A model for the SAR mode altimeter waveform derived in the SAMOSA project, which includes non_Guassian ocean wave statistics, the effects of earth curvature.
SAMOSA+	An implementation of the SAMOSA2 re-tracker modified for coastal application
SAR	Synthetic Aperture Radar
SARIn	Synthetic Aperture Radar Interferometric
SIRAL	SAR Interferometric Radar Altimeter
SLA	Sea Level Anomaly
SoW	Statement of Work
SSB	Sea State Bias
SSH	Sea Surface Height
SWH	Significant wave height
TAI	Temps atomique international (International Atomic Time)
TDP	Thematic Data Product
TEC	Total electron content
UTC	Coordinated Universal Time
WGS84	World Geodetic System 1984

Table of Contents

1 INTRODUCTION

1.1 Purpose and Scope

This document comprises the Algorithm Theoretical Basis (ATBD) for the coastal ocean algorithm used for the *CryoSat-2 ThEMatic PrOducts* (*Cryo-TEMPO*) study, Ref: ESA AO/1-10244/2-/I-NS. The ATBD has been written by the coastal ocean team led by the Collecte Localisation Satellite, with contributions from all members of the Cryo-TEMPO consortium. Lancaster University as the prime contractor is the contact point for all communications regarding this document.

1.2 Document Structure

This document provides a high-level description of the algorithms and processing used to produce each Cryo-TEMPO coastal ocean product parameter. The document is structured as follows:

- **Section 1 – Introduction**
- **Section 2 – Coastal Ocean Parameters**
- **Section 3 – Overall Coastal Ocean Processing Flow**
- **Section 4 – Algorithm Description**
- **Section 5 – Examples**
- **Section 6 – Known Issues**

1.3 Applicable and Reference Documents

Applicable documents

Reference	Title
AD1	Statement of Work ESA Express Procurement Plus - EXPRO+ CryoSat-2 ThEMatic PrOducts | Cryo-TEMPO, Issue 1, Revision 0, Date of Issue 01/04/2020 [Ref. ESA-EOPG-EOPGMQ-SOW-10].
AD2	Invitation to Tender for CryoSat-2 ThEMatic PrOducts | Cryo-TEMPO REF.: ESA AO/1-10244/2-/I-NS [Ref. SA-IPL-POE-NS-sp-LE-2020-313].
AD3	Draft Contract, CryoSat-2 ThEMatic PrOducts | Cryo-TEMPO, Appendix 2 to ESA AO/1-10244/20/I-NS.

Reference documents

Reference	Title
RD1	CryoSat Product handbook. Baseline-D Version 1.1 (https://earth.esa.int/documents/10174/125272/CryoSat-Baseline-D-Product-Handbook)
RD2	Baseline-C CryoSat Ocean Processor, Ocean Product handbook. Version 4.1 (https://earth.esa.int/documents/10174/125272/CryoSat-Baseline-C-Ocean-Product-Handbook)

2 COASTAL OCEAN PARAMETERS

2.1 Parameter Definition

This section describes the main parameters contained in the Cryo-TEMPO Coastal Ocean thematic data product (TDP).

Cryo-TEMPO coastal ocean products contain **measurements along the track** (at 20 measurements per second) of the CryoSat orbit and are not gridded.

Parameter	Description	Units
Time	UTC time of measurement acquisition	s
Latitude	Latitude of estimated echo location (point of closest approach) [-90,+90]. Positive latitude is North latitude, negative latitude is South latitude.	degs (N)
Longitude	Longitude of estimated echo location (point of closest approach) [-180,+180]. East longitude relative to Greenwich meridian.	degs (E)
Sea level anomaly (SLA)	Measured height of the sea surface with respect to the reference mean sea level (CNES/CLS2015) at the coordinate location [lon_poca_20_ku] [lat_poca_20_ku], computed via the SAMOSA+ retracker. All instrumental and appropriate geophysical corrections included.	m
Absolute dynamic topography (ADT)	Measured height of the sea surface above the reference geoid (EIGEN-6C4 model) at the coordinate location [lon_poca_20_ku] [lat_poca_20_ku]. This is computed as the sum of the estimated SLA and the reference Mean Dynamic Topography (MDT; MDT_CMEMS_2020_MED).	m
Filtered SLA	Smoothed SLA by applying a low-pass Lanczos filter	m
Filtered ADT	Smoothed ADT by applying a low-pass Lanczos filter	m
SLA Uncertainty	Contains an estimate of the uncertainty of each SLA measurement.	m
ADT Uncertainty	Contains an estimate of the uncertainty of each ADT measurement.	m
Filtered SLA uncertainty	Contains an estimate of the uncertainty of each filtered SLA measurement.	m
Filtered ADT Uncertainty	Contains an estimate of the uncertainty of each filtered ADT measurement.	m
Measurement Mode	The mode the CryoSAT SIRAL instrument was in when each measurement was taken (LRM, SAR)	flag
Valid Flag	Flag indicating if the altimeter measurement is considered valid or not	flag
Distance from the coast	Distance of each observation from the closest coastline point based on the GSHHG database (https://www.soest.hawaii.edu/pwessel/gshhg/)	m

2.2 Target Audience and Intended Use

The target audience for Cryo-TEMPO thematic coastal ocean product are satellite altimetry expert and non-expert users who require access to sea level observations from CryoSat at full resolution and with processing steps and assumptions specific for the coastal region.

Potential use cases include:

1. Regional analysis of sea level rise and direct comparison with tide-gauge in-situ measurements.
2. Assimilation in operational ocean models.
3. Integration in level-4 multi sensor products to generate gridded fields of sea surface height and surface geostrophic currents.

3 OVERALL COASTAL OCEAN PROCESSING FLOW

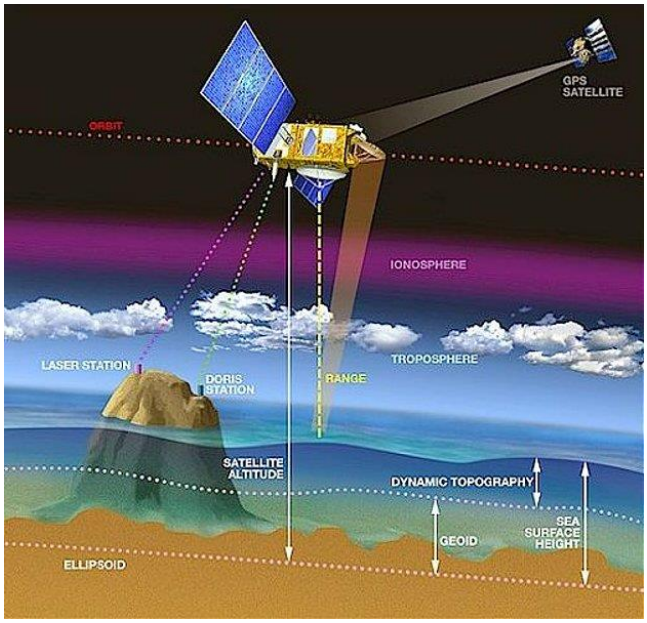

Figure 1: Schematic of the principle to retrieve sea surface height from CryoSat-2 altimeter observations (*image from https://www.aviso.altimetry.fr/en/techniques/altimetry/principle/basic-principle.html*)

3.1 General principles of satellite altimetry

The measurement retrieved from the altimeter is the 'Altimeter Range', which is the distance between the center of mass of satellite to the surface of the Earth (see Figure 1). The process to obtain the 'Altimeter range' from the recorded waveforms is called retracking. The 'Sea Surface Height' (SSH, the height of the sea surface above the reference ellipsoid) is then computed by combining the measured range with the 'Satellite Altitude' (the distance of the center of mass of the satellite above the ellipsoid) and a series of corrections to take into account various effects of specific environmental conditions:

$$SSH = Satellite\ Altitude - Altimeter\ Range - Corrections$$

These environmental corrections include atmospheric propagation corrections and ocean surface corrections. All corrections applied for the production of the CO TDP are listed in Table 1.

The Mean Sea Surface (MSS) is the temporal mean of the SSH over a given period. It represents the mean surface above the ellipsoid of reference and it includes the Geoid.

$$MSS=\langle SSH \rangle$$

The Sea Level Anomaly (SLA) is the anomaly of the SSH around the mean component, and it is thus computed as:

$$SLA = SSH - MSS$$

The Mean Dynamic Topography (MDT) is the temporal mean of the SSH above the Geoid.

$$MDT = MSS - Geoid$$

The Absolute Dynamic Topography (ADT) is the instantaneous height above the Geoid. The geoid is a gravity equipotential surface that would correspond with the ocean surface if ocean was at rest (i.e. with no currents under only the gravity field). When the ocean is also influenced by wind, differential heating and precipitation and other sources of energy, the ocean surface departs from the geoid. Thus the ADT provides information on the ocean dynamics. The ADT is the sum of the SLA and MDT:

$$ADT= SLA + MDT = SSH - MSS + MDT$$

3.2 Current issues in coastal altimetry

Altimetry observations within the coastal region (corresponding to a first approximation to the first 100 km off the coast) are a key source of information to better understand the rate and variability of sea level rise in different regions of the world as well as the complex ocean dynamics characterizing those environments. Traditional nadir altimetry is limited in the coastal zone by two main factors: a) degradation of the received signal due to spurious land reflections; b) insufficient resolution to observe coastal processes which are often characterized by smaller spatio-temporal scales compared to the open ocean ones. CryoSat-2 SIRAL altimeter has a smaller footprint, higher spatial resolution and reduced noise compared to traditional altimeters. Thus, CryoSat-2 observations have the potential to provide improved remote sensing coverage and accuracy near the coast. However, the full potential of CryoSat-2 observations within the coastal zone is currently not exploited since the CryoSat-2 processing chain is optimized for the open ocean. The goal of the Cryo-TEMPO Coastal Ocean TDP is to further enhance the quality and performance of CryoSat-2 coastal observations by implementing a processing chain with state of the art corrections and parametrizations specific for the coastal environment. Currently these include the implementation of:

- SAMOSA+ retracker for SAR waveforms (Section 4.2).
- Regional tidal model (Section 4.3.2.3).
- SSB correction at 20Hz (Section 4.3.2.6).
- High-frequency adjustment correction for LRM observations (Section 4.3.2.7).
- Regional mean dynamic topography for a more accurate reconstruction of local dynamics (Section 4.3.3.2).
- Novel iterative editing for the identification of outliers based on the local characteristics of the altimetry signal (Section 4.4).
- Dedicated uncertainty estimation (Section 4.6)

All corrections and parametrization will be regularly improved in future versions of the TDP.

3.3 Region of focus of the Coastal Ocean TDP

The CO TDP will be mainly based on the baseline CryoSat-2 L1b and L2 SAR and LRM products, and will span from 16 July 2010 until present. In the second phase of the project the TDP will cover exclusively the Mediterranean and Black Sea region (between -6.4 to 42 longitude, and 30 to 47.5 latitude; Figure 2). SARIn observations are currently not processed to generate the TDP since they require a specific implementation and tuning of the SAMOSA+ retracker. They can be included in future versions of the dataset, to improve the coverage after December 2015, when regions of SARIn acquisition were introduced over the Aegean sea and the Northern Italian region.

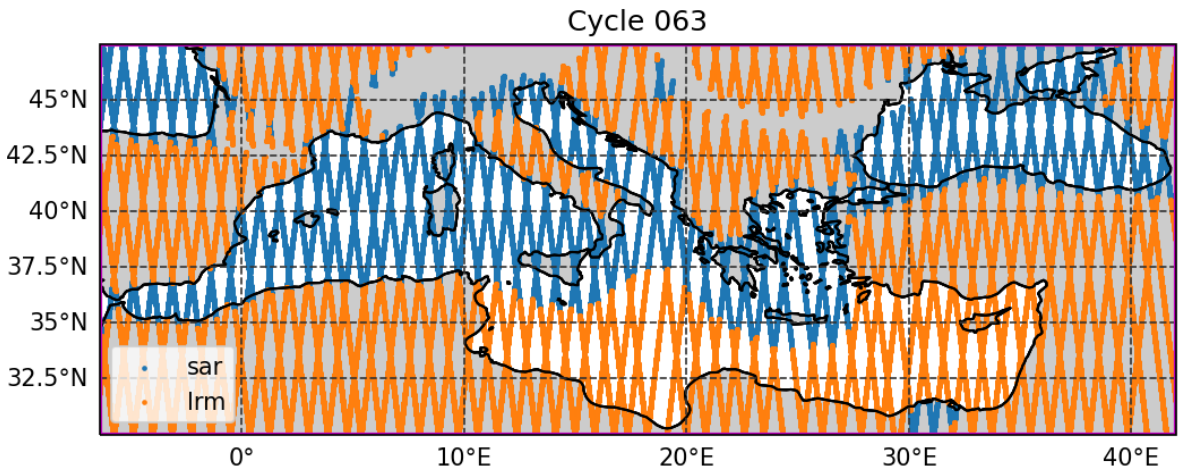

Figure 2: CryoSat-2 track over the Mediterranean basin for cycle 63. In blue are the tracks collected in SAR mode; in orange those collected in LRM. The python implementation of the SAMOSA+ retracker within Cryo-TEMPO will be applied, and thus tested, only over the SAR tracks.

3.4 Cryo-TEMPO Coastal Ocean Processing Chain

The processing chain used to compute Coastal Ocean SLA and ADT is broken down into several distinct sub-steps (Figure 2):

1. Estimate radar range for each waveform of the different surface types (**retracking**).

2. Apply environmental **corrections**:
    a. Atmospheric corrections (i.e. due to varying radar wave propagation speed in the iono- and troposphere).
    b. Ocean surface corrections (i.e. remove of the effect of tides and waves on the along-track elevations).
    c. Reference surface (i.e. MSS and MDT to compute SLA and ADT, respectively).

3. Identify and retain only the valid SSH measurements (**editing**).

4. Combine the SAR and LRM granules in a single netcdf file for each track.

5. Apply a Lanczos filter to compute low-pass, smoothed SLA and ADT and estimate uncertainties.

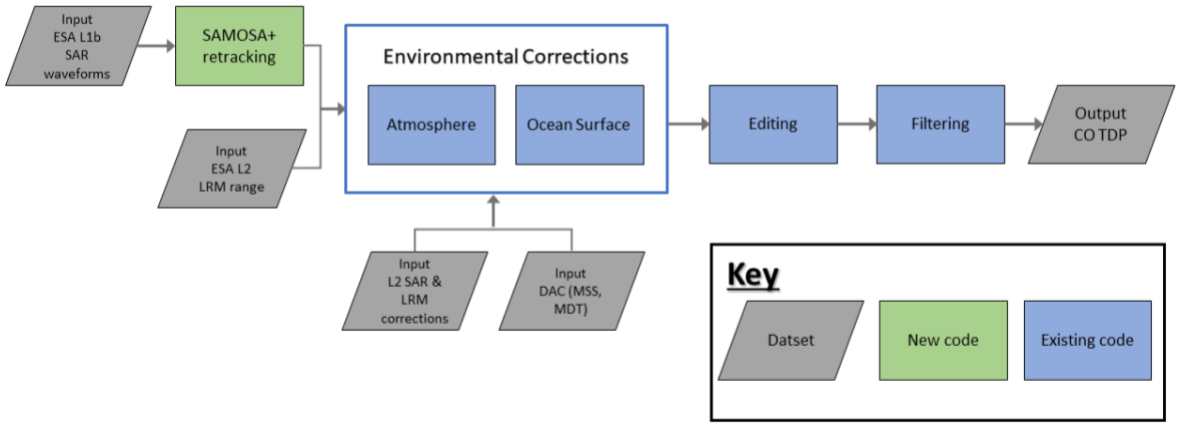

Figure 2: Processing workflow of geophysical retrieval of SLA and ADT for the Cryo-TEMPO Coastal Ocean product.

3.4.1 The CO TDP "time" variable

The CO TDP consist of a series of netcdf files for each individual CryoSat-2 track. To build each file, SAR and LRM observations along a given track are combined together. Observations for each mode maintain their original time variable from the corresponding GOP L1b and L2 product. Thus the variable "time" within the CO TDP product consist of the variables "time_20_ku" from the LRM L2 product and "time_20_hr_ku" from the SAR L1b products concatenated together (the latter is converted from international atomic time (TAI) to coordinated universal time (UTC)). Because of that, the "time" variable in the CO TDP is characterized by:

a) Gaps at the interface between the two modes, due to the instrument turning on and off to switch from SAR to LRM and vice versa.
b) Irregular spacing, since although the original "time_20_hr_ku" and "time_20_ku" variables are both sampled at 20Hz, they are not aligned with each other.

For more information please refer to the official CryoSat-2 Product Handbooks [RD1 and RD2].

Corrections and reference surfaces	Standard	Description
Wet troposphere	GPD+	Correction for the path delay in the altimetric return signal due to water vapor in the atmosphere [RD1]
Dry troposphere	ECMWF	Correction for refraction due to the dry gas component of the atmosphere [RD1]
Ionosphere	GIM	Correction for the free electrons in the Earth's ionosphere slowing the radar pulse [RD1]
Altitude	WGS84	Satellite elevation with respect to the reference ellipsoid [RD1]
Retracker (SAR)	**SAMOSA+**	Evolution of the SAMOSA2 retracker with enhanced performance in coastal regions [Dinardo et al., 2018]
Retracker (LRM)	MLE4	Altimeter waveform MLE retracker with 4 free parameters estimated [RD1]
Solid earth tide	Cartwright model	Correction for the deformation of Earth's body due to tidal forces [RD1]
Ocean tide	**RegAT-Med regional model**	Correction for the sea surface height amplitude due to ocean tide [Cancet et al. 2022]
Pole tide	**Desai 2015 with 2017 mean pole location**	Correction for the long-period distortions of the Earth's crust due to variations in centrifugal force as the Earth's rotational axis moves its geographical location [Desai et al., 2015]
DAC	MOG2D	Correction for the depression of the ocean surface due to local barometric pressure and wind effects [RD1]
SSB	**Tran 2018**	Correction for the intrinsic bias due to the large footprint radar measurements and dependent on swell and wind conditions at the sea surface. [Tran 2018]
HFA	**Tran 2019**	Correction for the correlation between significant wave height (SWH) and range errors in the retracked range. Only appliet to LRM observations. [Tran et al., 2019]
MSS	**Composite (DTU, SCRIPPS,CNES-CLS15)**	Anomaly of the SSH around its temporal mean component above the reference ellipsoid (WGS84) [Lievin et al., 2020]
MDT	**CMEMS_2020_MED**	Temporal mean of the SSH above the Geoid (EIGEN-6C4 model) [CMEMS]
Editing	**Iterative**	Selection of valid data according to user-defined criteria
Filtering	**Lanczos low-pass**	Applied to remove the high frequency content (instrumental noise) [Taburet et al., 2019]

Table 1: List of correction and processing algorithm used to compute the Cryo-TEMPO coastal ocean TDP. In bold are the components different from the official Geophysical Ocean Product (GOP) Baseline C products.

4 ALGORITHM DESCRIPTION

This section provides a description of the various steps from Figure 2 required for the generation of the Cryo-TEMPO coastal ocean thematic product. As the SAMOSA+ retracker represents the most significant difference with respect to the GOP product, baseline C and the python version used in Cryo-TEMPO is entirely new and specifically implemented for the project, particular attention will be dedicated to its thorough description.

4.1 Source Data

Input data to the coastal ocean processing algorithm falls into two categories:

1. Primary data: Radar altimeter data from the CryoSat's SAR Interferometric Radar Altimeter (SIRAL).
2. Auxiliary data: External data sets aiding the calibration or geophysical retrieval.

Each data set is described in corresponding sections below.

4.1.1 CryoSat-2 altimeter data

The primary input data to the Cryo-TEMPO thematic coastal ocean product is Level-1b data from the ESA CryoSat-2 baseline-C GOP processing chain for LRM and SAR radar modes. The files are delivered as one netCDF file separated by changes of the radar mode. Information about the CryoSat-2 products of the GOP processor can be found on RD2.

4.1.2 Auxiliary Data

Auxiliary data sets are data sets that are input to the geophysical retrieval but are not a measurement of the CryoSat-2 radar altimeter. Auxiliary data sets can be static fields or data sets from satellite observations with variable temporal coverage and resolution.

Auxiliary data currently used for the production of the CO TDP include the Oceanic Tide (See section 4.3.2.3), Mean Sea Surface (MSS) and Mean Dynamic Topography (MDT) (See section 4.3.3) as well as the LUT for the SSB and HFA corrections (sections 4.3.2.6 and 4.3.2.7, respectively).

4.2 Retracker

The retracker used for generate the Cryo-TEMPO coastal ocean TDP is SAMOSA+ (Dinardo et al. 2020). A python implementation of the retracker has been specifically implemented within Cryo-TEMPO. This version will be also used to generate other thematic products (i.e. land and polar ice, polar ocean and inland waters) in the second phase of the project.

The python source code for the SAMOSA+ retracker is publicly available under GPL-3.0 license at the following github repository: https://github.com/cls-obsnadir-dev/SAMPy

4.2.1 SAMOSA Analytical SAR (Delay-Doppler) Return Waveform Model

The expression of the SAMOSA analytical model as function of the beam look angle and waveform time-delay is given by Ray et al. (2015) and reformulated by Dinardo (2020) as:

$$P_{SL}(\theta_{Look}, t-t_0) = P_u \cdot \frac{\sqrt{2\pi}\cdot\alpha_p^2}{\sqrt{\mathrm{B_r}}} \cdot \frac{\Gamma_{k\ell}(0)}{\sqrt{\sigma_c}} \cdot \left[f_0\left(\frac{t-t_0}{2\sigma_c}\right) + \frac{\sigma_z}{L_\Gamma}\cdot T_k \cdot g_\ell \cdot \frac{\sigma_z}{\mathrm{L_z}} \cdot f_1\left(\frac{t-t_0}{2\sigma_c}\right)\right] \tag{4.2.1}$$

where:

$$f_0\left(\frac{t-t_0}{2\sigma_c}\right) = \frac{\pi}{2\sqrt{2}}\left|\frac{t-t_0}{2\sigma_c}\right|^{\frac{1}{2}}\left[I^{sc}_{-\frac{1}{4}}\left(\left(\frac{t-t_0}{2\sigma_c}\right)^2\right) + sign(t-t_0)\cdot I^{sc}_{\frac{1}{4}}\left(\left(\frac{t-t_0}{2\sigma_c}\right)^2\right)\right]$$

$$f_1\left(\frac{t-t_0}{2\sigma_c}\right) = \frac{\pi}{2\sqrt{2}}\left|\frac{t-t_0}{2\sigma_c}\right|^{3/2}\left[\left(I^{sc}_{\frac{1}{4}}\left(\left(\frac{t-t_0}{2\sigma_c}\right)^2\right) - I^{sc}_{-\frac{3}{4}}\left(\left(\frac{t-t_0}{2\sigma_c}\right)^2\right)\right) + sign(t-t_0)\cdot \cdot \left(I^{sc}_{-\frac{1}{4}}\left(\left(\frac{t-t_0}{2\sigma_c}\right)^2\right) - I^{sc}_{\frac{3}{4}}\left(\left(\frac{t-t_0}{2\sigma_c}\right)^2\right)\right)\right]$$

$$\Gamma_{k,\ell}(0) = exp\left[-\gamma_y(\theta^2_{Roll}) - \nu\cdot(\theta_{Look}-\theta_{Pitch})^2 - \gamma_x(\theta_{Look}-\theta_{Pitch})^2\right] \cdot \begin{cases} exp\left[-(\gamma_y+\nu)\left(\frac{c\cdot(t-t_0)}{\alpha h}\right)\right] cosh\left(2\gamma_y\theta_{Roll}\sqrt{\left(\frac{c\cdot(t-t_0)}{\alpha h}\right)}\right) & t > t_0 \\ 1 & t \le t_0 \end{cases}$$

$$T_k = \begin{cases} \left(1+\frac{\nu}{\gamma_y}\right) - \frac{\theta_{Roll}}{\sqrt{\left(\frac{c\cdot(t-t_0)}{\alpha h}\right)}} tanh\left(2\gamma_y\theta_{Roll}\sqrt{\left(\frac{c\cdot(t-t_0)}{\alpha h}\right)}\right) & t > t_0 \\ \left(1+\frac{\nu}{\gamma_y}\right) - 2\gamma_y\theta^2_{Roll} & t \le t_0 \end{cases}$$

$$g_\ell \cdot (k-k_0) = \frac{\tau}{\sqrt{\sigma_p^2\left[1+\left(\frac{\theta_{Look}}{\theta_{Lim}}\right)^2\right] + sign(SWH)\cdot\left(\frac{|SWH|}{2c}\right)^2}} = \frac{\tau}{\sigma_c}$$

$$\gamma_x = \frac{8 \cdot ln(2)}{\theta_x^2} \quad ; \quad \gamma_y = \frac{8 \cdot ln(2)}{\theta_y^2} \quad ; \quad L_\Gamma = \frac{\alpha \cdot h}{2\gamma_y}$$

$$L_x = \frac{ch}{2V_s f_c L_b} \quad ; \quad L_y = \sqrt{\frac{ch}{B_r \alpha}} \quad ; \quad L_z = \frac{c}{2B_r}$$

$$\theta_{Look} = \left(\frac{L_x}{h}\right)\ell \quad ; \quad \theta_{Lim} = \frac{L_z}{\alpha L_x} \quad ; \quad \tau = \frac{k-k_0}{B_r} = t - t_0$$

with symbols expressed in Table 2.

The representation of Eq. (4.2.1) in the time-delay/beam Doppler angle plane is referred to as Delay-Doppler Map (DDM).

Equation 4.2.1 is valid strictly in case the skewness of the ocean surface elevation distribution is assumed to be zero.

Equation 4.2.1 shows the explicit dependence of the model on the three altimetric unknowns (epoch t_0, SWH, P_u), on roll and yaw antenna mispointing angles and on the sea surface mean square slope.

Finally, the multi-looked SAR (Delay-Doppler) waveform model is provided by Equation 4.2.2:

$$P_{ML}(t - t_0) = \frac{1}{L} \cdot \sum_{\ell=-\frac{L}{2}}^{\frac{L}{2}-1} P_{SL}(\theta_{Look}, t - t_0)$$

where L is the total number of Doppler beams (i.e. looks) which have been accumulated.

Symbol	Description	Symbol	Description
SWH	significant wave height	θ_{Pitch}	antenna pitch mispointing
ℓ	Doppler beam index	θ_{Roll}	antenna roll mispointing
k	range bin index	B_r	receiver pulse bandwidth
t	fast time, defined as $t = \frac{k}{B_r}$	f_c	radar pulse carrier frequency
k_0	Waveform epoch range bin index	N_p	number of radar pulses in a transmitted burst
t_0	waveform epoch, defined as $t = \frac{k_0}{B_r}$	PRI	pulse repetition interval

τ	Waveform time delay, defined as: $\tau = t - t_0$	L_b	Burst duration, defined as: N_p ·PRI
P_u	waveform amplitude	c	speed of light
θ_{Look}	Doppler beam look angle	σ_z	ocean surface roughness, defined as: σ_z=SWH/4
L	total number of accumulated Doppler beams	s^2	mean square slope of the sea surface
σ_c	sigma composite	ν	inverse of the mean square slope of the sea surface, defined as: $\nu = \frac{1}{s^2}$
L_x	along track resolution	R_{EARTH}	local Earth radius
L_y	pulse-limited radius	h	orbit altitude of the satellite center of mass
L_z	vertical resolution	V_s	satellite center of mass velocity
π	Greek pi	α	Earth roundness coefficient, defined as: α=1+(h/R_{EARTH}),
σ_p	PTR time width, defined as $\sigma_p = \frac{\alpha_p}{B_r}$	$sign(\xi)$	sign function defined as: $sign(\xi) = \frac{\xi}{\lvert\xi\rvert}$
α_p	dimensionless PTR width	I_{nu}	Modified Bessel function of first kind and order nu
θ_x	3dB antenna aperture in along-track direction	I_{nu}^{sc}	Scaled Modified Bessel function of first kind and order nu, defined as: $I_{nu}^{sc}\left(\frac{1}{4}\xi^2\right) = e^{-\frac{1}{4}\xi^2} \cdot I_{nu}\left(\frac{1}{4}\xi^2\right)$
θ_y	3dB antenna aperture in across-track direction	$\lvert\xi\rvert$	absolute value function
N_s	number of range bins in the waveforms	$round(\xi)$	round function to nearest integer

Table 2: List of Symbols with description

4.2.2 SAMOSA (Open Ocean) Retracker

The SAMOSA waveform model has been implemented as an open ocean SAR (Delay-Doppler) retracker with the following characteristics:

- Usage of LUT for the α_p parameter in the σ_c term

- mean square slope set to infinite
- tabulation of f_0 and f_1 functions
- Constrained Least-Square Estimator (LSE) using Levenberg-Marquard approach or Trust-Region approach
- Model Zero-Masking by exact range shifts (once given in input)
- Model evaluated at the exact look angles (once given in input)
- Thermal Noise from the waveform's early samples
- Mispointing Angles as input from the star trackers
- Treatment of Hammimg-weighted waveforms via separate α_p LUT

4.2.2.1 α_p LUT

The SAR multi-looked return waveform model in its final formulation (Eq. 4.2.1) approximates the instrument point target response (PTR, which theoretically is a sine cardinal squared function) with a Gaussian curve having a shape-factor coefficient α_p:

$$\mathrm{sinc}^2(x) \approx e^{-\left(\frac{x}{\sqrt{2}\alpha_p}\right)^2}$$

(4.2.3)

The above approximation is expected to lead to sea-state related errors in range and significant wave height which are not negligible (Fenoglio-Marc et al., 2015). In order to mitigate those errors, it has been conceived to build a look-up table of this α_p parameter for a different conditions of sea state regime, making a model-model fitting (as in Fenoglio-Marc et al., 2015). The models to be fitted are the numerical SAMOSA model (wherein the approximation (4.2.3) is not done and is considered the "reference model") and the SAMOSA analytical model expressed above by equation 4.2.1.

The α_p LUT is meant to be applied at run time, (i.e. during the re-tracking algorithm execution), extracting, from the table, the α_p value corresponding to the SWH value under iteration.

Because it has been computed after normalizing the analytical and numerical SAMOSA model, it is supposed to not have any effect on the retracker power. Hence it is used only inside the sigma composite σ_c term whereas for the α_p parameter next to Pu in Eq. 4.2.1 a constant value is used. This value has been computed as to be about 0.5, making a cross-comparison between the analytical and numerical SAMOSA model power for the same epoch and SWH equal to 2 meter.

The α_p LUT needs to be recomputed for a new or other missions since it depends on the geometry scenario and sensor parameters.

4.2.2.2 Mean Square Slope set to infinite

In the SAR open ocean retracker as used in (Fenoglio-Marc et al., 2015), the mean square slope has been set to infinite, i.e. the parameter v gets set to zero. This position of the mean square slope set to infinite means that the ocean surface is considered an infinitely diffusive surface over the antenna footprint. Hence the backscattering profile of the ocean surface at near-nadir incidence of the altimeter is assumed to be uniform and not depending on the look angle.

4.2.2.3 Tabulation of f_0 and f_1 functions

Even if the f_0 and f_1 functions in Eq. 4.2.1 are expressed in closed form and there are open source implementations of Scaled Bessel Function (see GNU Scientific Library (GSL) freely distributed under GNU GPL license), it has been decided to make a tabulation of the f_0 and f_1 functions versus the argument ξ and to read this tabulation at run time in order to evaluate the model's equation. The reason for this was to make the retracking computationally as fast as possible. Furthermore, these tabulations are not depending on any sensor parameters (the sensor parameter enter solely in the argument ξ) and hence they do not need to be recomputed for new or others missions. Finally, for high values of the argument ξ (more than 9), the following asymptotic approximation for f_0 has been used:

$$f_0(\xi) = \sqrt{\frac{\pi}{2}} \cdot \frac{1}{\sqrt{\xi}} \left[1 + \frac{3}{8} \cdot \frac{1}{\xi^2} + \frac{105}{128} \cdot \frac{1}{\xi^4}\right]$$

For $\xi > 6$, the difference between the exact solution and the approximated one is lesser than 1e-4. Similarly, for high values of the argument ξ, the f_1 function has been approximated by its asymptotic formulation:

$$f_1(\xi) = \sqrt{\frac{\pi}{8}} \cdot \frac{1}{\sqrt{\xi^3}}$$

4.2.2.4 Least Squares Estimator with Levenberg-Marquardt approach (LSE-LM) or Trust Region approach (LSE-TR)

The LSE algorithm (Least Squares Estimator) is a minimization technique of a function F(x) (referred as objective function) which is sum of squares of M non-linear functions f_i:

$$F(x_k) = \frac{1}{2} \sum_{i=1}^{M} [(f_i(x_k))]^2 \qquad (4.2.4)$$

Where M is the total number of non-linear functions f_i, each of them has x_k independent variables.

Denoted as $J_i(x_k)$ the Jacobian of $f_i(x_k)$, then the LSE-LM (Levenberg-Marquardt) searches the solution δ_k of the equation:

$$(\boldsymbol{J}_k^T\boldsymbol{J} + \lambda_k\boldsymbol{I})\delta_k = -\boldsymbol{J}_k^T\boldsymbol{f}_k$$

where λ_k are non-negative scalar and I is the identity matrix. The factors λ_k are known as damping factors and usually are taken identical for all the k unknowns of the problem.

In our altimetry case, the function f_i in Eq. (4.2.4) are the residuals between waveform data and waveform model while δ_k are the deviations from the truth x_k for our retracked variables. Our retracked (unknown) variables are three: epoch, SWH and Pu.

The LSE-LM can be imagined as a generalization of the classic LSE-GN (Least Squares Estimator with Gauss-Newton approach) which searches the solution δ_k of the equation:

$$(\boldsymbol{J}_k^T\boldsymbol{J})\delta_k = -\boldsymbol{J}_k^T\boldsymbol{f}_k$$

and therefore LSE-LM is usually referred also as damped Least-Squares Estimator.

It can be demonstrated that the LSE-LM:

- does not have a specific direction search.
- for very low value of the damping factors, it reduces to Gauss-Newton approach while for high values of the damping factor it tends to behave as Descent Gradient Method .

An initial value λ of the damping factor is needed to be passed in input to the algorithm. This value is then internally updated by the algorithm at each iteration using the gain ratio formula. If the reduction of the sum of the squared residuals is fast and the algorithm gets close to the solution, the damping factor undergoes only small changes or it gets reduced whereas, if the reduction is not achieved and algorithm is far from the solution, the algorithm automatically increases the value of the damping factor to accelerate the convergence and the direction search will be nearly the gradient direction (which is good if the current iteration is far from the solution). Hence LSE-LM is an adaptive algorithm because it controls its own damping.

The LSE Trust Region (LSE-TR) is a further evolution of the LSE Levenberg-Marquardt.
In a trust region LSE, the solution δ_k are now the solutions of the problem:

$$\mathcal{L}(\delta_k) = \min_{\delta_k} Q(\delta_k) \quad \text{subject to} \quad \|\delta_k\| < \Delta$$

where:

$$Q(\delta_k) = F(x_k) + g_k^T \delta_k + \frac{1}{2}\delta_k^T B_k \delta_k$$

is the the quadratic (i.e. second order) approximation of $F(x_k)$ around x_k , g_k is the gradient of $F(x_k)$ computed at x_k , B_k is an approximation of the hessian matrix H_k of $F(x_k)$ at x_k and Δ is a positive scalar representing the radius of the trust region which is a spherical zone in the neighbourhood centered around the point x_k.

The algorithm updates the current point to $x_k + \delta_k$ if $F(x_k+\delta_k) < F(x_k)$, i.e. it accepts the update, it remains in the same region or enlarges the region in case the objective Function is reduced after the iteration; otherwise (that means Q was an ill-conditioned approximation of $F(x_k+\delta_k)$), the current point remains unchanged and the algorithm shrinks the trust region (in order to improve the approximation Q of $F(x_k+\delta_k)$ and then repeats the trial step δ_k computation.

The key point of a trust region algorithm is how to compute the trust region trial radius and how to decide whether a trial step δ_k should be accepted. An iteration of a trust region algorithm has the following scheme: a trust region is available at the beginning, then an approximate model of the objective function is constructed, and it is solved within the trust region, giving a solution δ_k which is the trial step. A merit function is chosen, which is used for updating the next trust region and for choosing the new iterate point.

A trust region algorithm for nonlinear least squares can be shown to work in a similar fashion to the Levenberg-Marquardt method, except that the radius Δ is updated from iteration to iteration instead of the parameters λ_k. Trust region algorithms are reliable and robust, they can be applied to bad-conditioned problems, and they have very strong convergence properties.

As far as it concerns the customization of the algorithm for our waveform's fitting, in order to avoid rounding problems inside the minimization process, the epoch has been expressed in nanoseconds while both the waveform data and the waveform model are normalized in order to make the waveform data and waveform model close to each other in amplitude.

Anyhow, it is important to bear in mind that LSE will find only a local minimum which will not be necessarily a global minimum. As consequence, it is fundamental to initialize properly the estimator to ensure a fast convergence. For the open ocean retracker, it has been set as first guess value:

- the maximum point of the waveform data for the epoch, knowing that the true epoch is very close to maximum point of the waveform.
- 2 meter for SWH, being most typical value of SWH.
- 1 for Pu, being the true Pu very close to the waveform's maximum.

Furthermore, for each of the retracked variables some constrains have been placed in order to avoid non- physical solutions.

These upper and lower values of the used constrains are:

	Epoch	SWH	Pu
lower bound	first sample of the epoch array	-0.5 meter	0.2
upper bound	last sample of the epoch array	20 meter	1.5

Table 3: Constraints (lower and upper bound for epoch, SWH and Pu).

Both estimator LSE-TR and LSE-LM are available in the python library scipy as least_squares method (https://docs.scipy.org/doc/scipy/reference/generated/scipy.optimize.least_squares.html). By default, LSE-TR is chosen since is considered superior to LSE-LM. LSE-LM may be chosen following the user preference given in input.

4.2.2.5 Model Zero-Masking by exact or approximated range shifts

Due to the limited size of the radar receiving window (around 60 meters), after the range cell migration process, the Doppler beams in the stack get padded with zeroes or with place-holder as NaN (Not a Number). Hence in order to maintain the consistency between model's Delay-Doppler Map (DDM) and stack data, it is necessary to compute from the stack a bitwise mask (1/0) giving the position of the pixels in stack data matrix wherein the zeroes are located and then apply this mask during the retracking to place the zeroes in the model's DDM.

If this zero-mask, constructed using the total applied range shift (sum of slant range shift, tracker range shift and Doppler range shift), has been computed at L1b in the process to align in range the Doppler beams, then it can be passed in input to the SAMOSA retracker (i.e. exact masking approach).

Specifically, the SAMOSA model's DDM values are replaced by zeros in the pixels (ℓ, k) where:

$$\Delta \mathrm{R}_{\ell} \geq \mathrm{R}_{\mathrm{k}}$$

with $\Delta \mathrm{R}_{\ell}$ is the applied total range shift and R_{k} is given by:

$$\mathrm{R}_{\mathrm{k}} = \Delta \mathrm{R} \cdot [N_s - 1 : -1 : 0]$$

where ΔR is the range bin width, N_s is the number of range bins, and [a:s:b] denotes an array starting from a until b with step s.

In case this total applied range shift is not available and not passed in input, the SAMOSA retracker builds a rough approximation of it, by the formula:

$$\Delta R_{\ell} = h \cdot \left\{ \sqrt{1 + \left[\alpha \cdot \left(\frac{\ell \cdot L_x}{h} \right)^2 \right]} - 1 \right\}$$

In this case, we speak of approximate zero-masking approach.

4.2.2.6 Model Evaluated at exact look angles

One of the inputs necessary to the SAMOSA model evaluation are the look angles. In order to be fully consistent with the L1b stack data, the look angles used in input to the SAMOSA model are the ones computed at L1b stage from the burst center and range locations positions (i.e. exact look angles). These look angles are then passed in input to the SAMOSA retracker.

The look angles theoretically have an angular separation of:

$$\Delta\theta_{Look} = \frac{V_s \cdot BRI}{h \cdot \alpha}$$

with:

$$\alpha = 1 + \frac{h}{R_{Earth}}$$

where V_s is the satellite center of mass velocity, BRI is the Burst Repetition Interval (around 11.79 ms for CryoSat-2), h is the satellite altitude and R_{Earth} is the mean Earth radius.

Converting this angular separation in Doppler frequency separation by:

$$\Delta f_{dop} = \frac{2 \cdot V_s \cdot BRI}{\lambda_0} \sin(\Delta\theta_{Look}) \quad (4.2.5)$$

where λ_0 is the pulse carrier wavelength (i.e. speed of light divided by pulse carrier frequency), one can see how the Doppler frequency step size given by Eq. 4.2.5 is lower than the sampling Doppler frequency given by:

$$\Delta f_{samp} = \frac{PRF}{N_p} \quad (4.2.6)$$

where N_p is the number of pulses in a burst (64). Hence, if one evaluates the DDM for all the look angles, it means that one is oversampling the DDM, i.e. evaluating it with a Doppler frequency

resolution lower than it was physically sampled by PRF. In order to reduce the computational time, the input look angles are converted to Doppler frequency by the formula:

$$f_{dop} = \frac{2 \cdot V_s}{\lambda_0} \cos(\theta_{Look})$$

Note that in our case θ_{Look} is assumed to be the angle with respect to the surface. Thus, it should be computed using the look angle from the L1b product as

$$\theta_{Look} = \frac{\pi}{2} - \theta_{Look\_product}$$

And then the rounded beam indexes ℓ are computed by the formula:

$$\ell = \frac{1}{f_{beam}} \cdot round\left(\frac{f_{dop} \cdot f_{beam}}{\Delta f_{samp}}\right) \quad (4.2.7)$$

where f_{beam} is an input factor, commanding the level of desired oversampling of the model DDM in the azimuth dimension ($f_{beam} = 1$ means no oversampling, as used in SAMOSA+ ; $f_{beam} > 1$ means oversampling of the DDM in azimuth).

In case $f_{beam} = 1$ the model Doppler beams have a frequency step given by Eq. 4.2.6 and the beam index ℓ in Eq. 4.2.7 will only take integer values. In case $f_{beam} > 1$, the beam index ℓ in Eq. 4.2.7 will take fractional values.

4.2.2.7 Thermal Noise from early samples

On top of the signal received from the surface, the waveform exhibits an additive random noise known as thermal noise (or better equivalent thermal noise) which can be considered as the sum of the radar receiver's electronic noise, atmospheric noise, the galactic noise and else.

In case of open ocean waveforms, because the on board tracker will place the waveform around the reference range gate, the waveform's early samples are just a measurement of this thermal noise level and generally are not influenced by signal reflected from the surface.

Hence, a very reliable and common technique to estimate the thermal noise floor from the waveform in pulse-limited altimetry is to compute the average of the waveform's early samples. This method was followed also in the SAR open ocean retracker in which the "noise range bins" used are [5,10].

4.2.2.8 Mispointing Angles as input from Star Tracker

Though the satellite attitude control subsystem has the task to ensure a platform attitude pointed to geodetic nadir, a perfect nadir-pointing can never be reached. Hence, each radar altimeter on board of a satellite will be slightly mispointed. In case of our SAR retracking, the mispointing angles (roll and

pitch) have been always derived from the satellite platform files (or L1A products) and injected in the retracker as input to the SAMOSA model. Hence, the mispointing angles are not estimated from the waveform in our approach and in general in SAR Altimetry. The rationale behind this is that there is a clear coupling (or cross-talk) between roll mispointing and SWH variables resulting both of them to have a very similar effect on the SAR waveform shape, making impossible for a SAR retracker to discriminate whether this effect has been triggered from a variation of SWH or a variation of the roll mispointing.

4.2.2.9 Treatment of Hamming-weighted Waveforms

In case the SAR waveform has been weighted at L1b in azimuth (for instance by Hamming window), a flag in the retracker configuration can command the reading of a different α_p LUT. This α_p LUT has been built with the same approach as presented in section 4.2.2.1 but now the numerical SAMOSA model (used in the process to build the LUT) has been generated weighting the azimuth PTR (Point Target Response) by the same Hamming window. Since the Hamming window also tapers the waveform power, in case this tapering is not compensated at L1b, it can be compensated via retracking changing the constant value of α_p term next to Pu in Eq. 4.2.1

4.2.3 SAMOSA+ (Coastal) Retracker

The SAMOSA-based open ocean retracker is expected to underperform over the coastal zone, inland water and sea ice wherein bright targets as sandbanks, off-nadir cliffs, ponds of still water, wetlands, water lead between ice floes, etc. etc. will break the assumption of incoherent backscattering surface on which the physical model bases. Even over open ocean, this retracker may sporadically fail to have a good fit to the waveform data because of oil slicks, ships and algae blooming events. In this section, we describe a way to generalize the SAMOSA-based open ocean retracker to any marine surface (at least) making usage of the mean square slope parameter and a better initialization of the retracker itself. This retracker is referred as SAMOSA+ and has been introduced in (Dinardo et al, 2018).

In case of SAMOSA+ retracker, the model in Eq. 4.2.1 has been implemented in the retracking scheme with two significant additions. The first one concerns the selection of the first-guess epoch. This is not selected anymore simply as the position of the waveform peak as in open ocean case but as the peak position of a moving point-wise product in a subset of 20 consecutive waveforms, after aligning them for tracker shift. Hence, the waveforms are first range-aligned for tracker shift using the quantity orbit altitude minus tracker range (these parameters are extracted from the L1b products).

Let W_n be the n-th range-aligned waveform: I consider a subset of 20 range-aligned waveforms formed by $[W_{n-10}, ..., W_n, ..., W_{n+9}]$ and I compute the point-wise product between the waveforms in the subset. The peak position of this point-wise product will be taken as first-guess epoch for W_n. This procedure is then repeated for all the waveforms in the pass. The rationale behind this choice is to attempt to mitigate the typical off-ranging effect in coastal data. Indeed, in the SAR open ocean retracking, the first-guess epoch is selected to be the epoch of waveform peak. This assumption that final retracked

epoch is sufficiently close to the SAR waveform peak is a valid one for open ocean conditions. In presence of off-nadir land contamination or off-nadir lead contamination, the afore-said assumption loses its validity because the maximum power can source as well from the off-nadir target. In this case, if the retracking is initiated with erroneous input information, the fitting very likely will converge to a fitting's relative minimum returning an incorrect value of the radar range. On the other side, the peak position of a moving point-wise product between range-aligned consecutive waveforms will represent a more robust and stable reference from which to start the fitting iterations and by which mitigate the off-nadir ranging effect impact. Hence, this enables a more reliable initialization of the retracking scheme in the coastal zone.

The second innovation concerns the treatment of land contaminated (or specular) waveforms. In case of waveforms deemed as not contaminated by land and diffusive, the SAMOSA model has been used with the inverse of the mean square slope set to zero, i.e. as described in the former section and in Fenoglio-Marc et al. (2015). For waveforms deemed as land contaminated (or specular), a two-step retracking approach is used: in the first step, the SWH is still estimated as in section 4.2.2 while in the second step, the SWH is set to zero and the third free parameter in the retracking becomes the mean square slope (as in Tseng et al. 2013 for pulse-limited altimetry and Kurtz et al. 2014 for SAR altimetry). The output of this second step is the range and the amplitude Pu and the mean square slope. This approach gives the capacity to the model to fit a very peaky waveform which arises from a bright target and to continue to fit the broad diffusive ocean waveforms as good as before. The continuity between the two steps is ensured by the fact that the same physical waveform model (SAMOSA) is used in both steps.

The quality parameter used to deem whether a waveform is contaminated by land or else is that just one of these conditions occurs:

$$\begin{cases} E \cdot PP < 0.68 \\ E \cdot PP > 0.78 \\ 100 \cdot PP \cdot zp > 4 \\ \dfrac{\mathrm{E}}{\mathrm{zp} \cdot \mathrm{misfit}} < 4 \end{cases} \tag{4.2.8}$$

where zp is the eventual zero-padding oversampling factor applied in range-compressing the waveform and E is the entropy of the waveform, defined as:

$$\mathrm{E} = -\sum_i (|\mathrm{W_i}|^2 \cdot \log 2(|\mathrm{W_i}|^2))$$

PP is the Pulse Peakiness, defined as:

$$\mathrm{PP} = \frac{\max(\mathrm{W_i})}{\sum_i (\mathrm{W_i})}$$

and W_i are the waveform samples whereas the misfit definition is reported in the equation:

$$\text{misfit} = 100 \cdot \sqrt{\frac{1}{N_s}\sum_i (\text{residuals}_i)^2}$$

where residuals are the differences between the modelled waveform and the data waveform for each waveform range bin, and N_s is the number of range bins. The values of the thresholds in equation 4.2.8 have been found in a heuristic manner.

Furthermore, it was stated that in the SAR open ocean retracker the SAMOSA SAR return waveform model is complemented by a Look-Up Table (LUT) of the α_p parameter to mitigate the effect of the model's approximation of the squared PTR with a Gaussian curve. The same α_p LUT keeps on being applicable also in case of SAMOSA+ retracker. In case the waveform is weighted by a Hamming window, a different α_p LUT (computed specifically for the Hamming-window weighting case) needs to be passed in input via retracker configuration. Since the Hamming window also tapers the waveform power, in case this tapering is not compensated at L1b, it can be compensated inside the retracker changing the constant value of α_p term next to Pu in Eq. 4.2.1.

The mask for the pixels padded to zero in the stack data after range cell migration is carried out in the SAMOSA DDM using the approximate zero-masking approach since the applied range shifts are not provided in the L1b GOP products. The SAMOSA model DDM is evaluated using the exact look angles computed at L1b stage and stored in the L1b GOP products. Regarding the thermal noise floor, since the waveform's early samples can get contaminated by off-nadir returns in the coastal zone, the usual technique to estimate it from the waveform early samples does not hold anymore. For this reason, in the SAMOSA+ retracker, since the thermal noise computed from the outer stack beams (as done in Dinardo et al, 2018) is not provided in the L1b products, the thermal noise is still computed from the waveform on a fixed window but, beforehand, the range bins of the waveforms have been re-sorted in an increasing order since the thermal noise (theoretically) is not depending on the order of the range bins. This approach helps to mitigate the possibility to have strong returns coming from land contamination in the range bins used to estimate the thermal noise level.

4.3 Corrections

This section describes all the corrections required to convert the measured range from the altimeter into SLA and ADT.

4.3.1 Atmosphere Propagation Corrections

Atmosphere propagation corrections are used to convert the altimeter range into corrected range (i.e. taking into account atmospheric path delay). These include wet tropospheric correction, dry tropospheric correction and the ionospheric correction.

4.3.1.1 Wet tropospheric correction

The Wet Tropospheric Correction (WTC) is the correction for the path delay in the altimetric return signal due to water vapor in the atmosphere. The water vapor in the troposphere is quite variable and produces a altimetric height calculation error of -6 cm to -40 cm. The Cryo-TEMPO Coastal Ocean product makes use of the WTC provided in the L2 CryoSat-2 Ocean Products (parameter **gpd_wet_tropo_cor_01)** based on the wet tropospheric delay provided by the ECMWF numerical weather prediction model. This correction is provided at 1 Hz and hence it is linearly interpolated to be applied to the 20 Hz Cryo-TEMPO observations.

4.3.1.2 Dry tropospheric correction

The Dry Tropospheric Correction (DTC) is the correction for refraction due to the dry gas component of the atmosphere, which generates a path delay in the radar return signal. The propagation velocity of a radio pulse is slowed by the "dry" gases and the quantity of water vapor in the Earth's troposphere. The Cryo-TEMPO Coastal Ocean product makes use of the DTC provided in the L2 CryoSat-2 Ocean Products (parameter **mod_dry_tropo_cor_01**) based on the surface pressure fields provided by the ECMWF numerical weather prediction model. This correction is provided at 1 Hz and hence it is linearly interpolated to be applied to the 20 Hz Cryo-TEMPO observations.

4.3.1.3 Ionospheric correction

The ionospheric correction compensates the free electrons in the Earth's ionosphere slowing the radar pulse. The Cryo-TEMPO Coastal Ocean product makes use of the ionospheric correction provided in the L2 CryoSat-2 Ocean Products (parameter **iono_cor_gim_01**) based on the Total Electron Content (TEC) grids computed from GPS-based observations and ionosphere model (the JPL Global Ionosphere Maps – GIM – model). This correction is provided at 1 Hz and hence it is linearly interpolated to be applied to the 20 Hz Cryo-TEMPO observations.

4.3.2 Ocean Surface Corrections

Ocean surface corrections are used to convert the corrected range into sea surface height. These include altitude, solid earth tide, ocean tide, pole tide, dynamic atmospheric correction, sea state bias and high frequency adjustment.

4.3.2.1 Altitude

The Cryo-TEMPO Coastal Ocean product makes use of the altitude provided in the L2 CryoSat-2 Ocean Products (parameter **alt_20_ku**). This altitude is interpolated from the satellite orbit at the exact time recorded in the timestamp. It is measured from the reference ellipsoid (WGS84, defined by the National Geospatial Intelligence Agency of the USA) at nadir to the satellite centre of gravity. The altitude is directly provided at 20Hz resolution.

4.3.2.2 Solid Earth Tide

The solid Earth tide correction removes the deformation of the Earth due to tidal forces from the Sun and Moon acting on the Earth's body. Typically, this correction ranges from -30cm to +30cm. The Cryo-TEMPO Coastal Ocean product makes use of the solid earth tide provided in the L2 CryoSat-2 Ocean Products (parameter **solid_earth_tide_01**) derived from the Cartwright model. This correction is provided at 1 Hz and hence it is linearly interpolated to be applied to the 20 Hz Cryo-TEMPO observations.

4.3.2.3 Ocean Tide

The oceanic tide correction contains the semi-diurnal, diurnal and Long Period (i.e. gravitational tides with periods longer than one day) tidal height – for a total of 34 constituents – as well as the Ocean Loading Tide (i.e. the deformation of the Earth due to the weight of the ocean tides). The Cryo-TEMPO Coastal Ocean product makes use of the RegAT-MET regional model ocean tide provided by Noveltis (Cancet et al., 2022, *in prep.*). The RegAT-Med regional model has been implemented in the framework of a project funded by CNES in preparation of the upcoming FES2022 global tidal model. Compared to the FES2014 global tidal model, the bathymetry has been improved in several regions. The resolution of the RegAT-Med model mesh grid ranges between 2 km at the coast and up to 16 km in the deep ocean. The model is constrained with data assimilation based on tide gauge and satellite altimetry tidal estimates. The RegAT-Med model is composed of 34 tidal components, like the FES2014 global tidal model. The ocean tide elevations are computed from the RegAT-Med regional model at each location and date of the CryoSat-2 measurements in the Mediterranean Sea. Since the loading tides are not included in the provided tidal elevations, they are retrieved directly from the L2 CryoSat-2 Ocean Products (parameter **load_tide_sol2_01**). As this parameter is provided at 1 Hz, the values are linearly interpolated to be applied to the 20 Hz Cryo-TEMPO observations.

4.3.2.4 Pole Tide

The geocentric polar tide correction removes a long-period distortion of the Earth's crust caused by variations in centrifugal force as the Earth's rotational axis moves its geographical location. Typically, this correction ranges from -2cm to +2cm. The Cryo-TEMPO Coastal Ocean product makes use of the solution based on Desai et al. 2015 which represent a further evolution with respect of the correction provided in the L2 CryoSat-2 Ocean Products -- i.e. accounts for self-gravitation, loading, conservation of mass, and geocenter motion (spatial dependence).

4.3.2.5 Dynamic Atmospheric Correction

The Dynamic Atmospheric Correction (DAC) corrects for the depression of the ocean surface caused by the local barometric pressure and wind effects. The Cryo-TEMPO Coastal Ocean product makes use of DAC provided in the L2 CryoSat-2 Ocean Products (parameter **hf_fluct_cor_01**). This correction is a combination of the high frequency, high resolution 2D Gravity Waves Model (MOG2D), an ocean model forced by ECMWF atmospheric parameters after removing S1 and S2 atmospheric tides, and the low frequency Inverse Barometric (IB) Correction. It is provided at 1 Hz and hence it is linearly interpolated to be applied to the 20 Hz Cryo-TEMPO observations.

4.3.2.6 Sea State Bias

The sea-state effects are an intrinsic property of the large footprint radar measurements. The sea state bias (SSB) is the sum of three different source of bias: the electromagnetic (EM) bias, the skewness bias, and the tracker bias. The EM bias is due to the unequal contributions of the different surface scattering elements to the radar return: troughs of waves tend to reflect altimeter pulses better than do crests, thus, the centroid of the mean reflecting surface is shifted away from mean sea level towards the troughs of the waves. This shift causes the altimeter to overestimate the range. The skewness bias exists from the assumption in the onboard algorithms that the probability density function of heights is symmetric, while in reality it is skewed. Finally, the tracker bias is a purely instrumental effect.

The accuracy of the SSB models remains limited and continues to be a topic of research. The current most accurate estimates are obtained using empirical models derived from analyses of the altimeter data. The sea state bias is computed from a bilinear interpolation of a table of sea state biases versus significant wave height and wind speed, based on empirical fits (Labroue et al. 2004). This is the same approach adopted for the Cryo-TEMPO SSB correction. For consistency, the Cryo-TEMPO SSB is computed at 20Hz for both SAR and LRM observations (since the LRM SSB from the L2 products is only provided at 1Hz). For SAR observations, SWH is provided directly by the SAMOSA+ retracker; for LRM observations it is the one from the L2 products (parameter **swh_ocean_20_ku**). For both modes the wind is derived from the backscatter coefficient sigma0 using the Abdalla 2012 method. For SAR observations sigma0 is provided directly by the SAMOSA+ retracker; for LRM observations it is computed by correcting (i.e. adding) the L2 backscattering coefficient (parameter **sig0_ocean_20_ku**) for the atmospheric attenuation (parameter **atm_cor_sig0_01** – this is linearly interpolated to 20Hz since it is only provided at 1Hz). SSB is then computed using the specific CryoSat-2 LUT defined for the CryoSat Ocean Processor (COP) (Tran et al. 2018). Although defined for CryoSat-2 SAR observations, these LUT are currently not specifically tuned for the SAMOSA+ retracker. A dedicated SAMOSA+ CryoSat-2 LUT is under development and will be included in future versions of the TDP.

4.3.2.7 High frequency adjustment

This is a novel additional correction applied to create the Cryo-TEMPO coastal ocean dataset. It is used to remove a significant source of noise which arise from the correlation between significant wave height (SWH) and range errors that is inherent to any traditional (i.e. non-SAR) waveform retracking algorithm (e.g. Quartly et al, 2019). As such the correction is only applied to LRM observations. The correlation is computed using an empirical model (in form of a LUT) that describe the relation between SWH and range. The model is specific for each satellite mission. Before being applied to the LUT, the SWH is filtered with a Lanczos-2 filter (with a cutoff wavelength of ~68 km – corresponding to a half-window width of 200 points). Via the LUT a portion of the SWH residual is converted into HFA correction based on the local values of filtered SWH. A more detailed description of the methodology used to produce the HFA correction for the Cryo-TEMPO coastal ocean dataset can be found in Tran et al (2019). Currently, the LUT parameters (as well as the Lanczos-2 filter cutoff length) have been

defined based on the observations from the Saral/AltiKa mission. Specific tuning for the CryoSat-2 observations over the Mediterranean will be developed and included in future versions of the TDP to avoid excessive smoothing of the SWH signal as well as minimize the slight degradation of the mesoscale SLA signal (roughly wavelengths above 50 km; this is an open known issue of the HFA correction).

4.3.3 Reference Surfaces

4.3.3.1 Mean sea surface

The MSS used to compute SLA is derived by combining the CNES-CLS15 used in coastal regions and high latitude areas), DTU15 (used in arctic regions north of 81°N) **and** SCRIPPS (used in open ocean) MSS. This MSS is currently not publicly available, but a brief description of its characteristics can be found in Lievin et al., 2020.

4.3.3.2 Mean dynamic topography

The MDT used to compute ADT is the latest Mediterranean MDT available from CMEMS, CMEMS_2020_MED. This represents an update of the MDT used to derive the L2 CryoSat-2 Ocean Products. A complete description of this MDT can be found here:
https://catalogue.marine.copernicus.eu/documents/QUID/CMEMS-SL-QUID-008-063-066-067.pdf

4.4 Editing

Editing is the selection of valid data. The Cryo-TEMPO coastal ocean thematic product will be based on a novel editing approach: as a first step, the 20Hz measurements are selected over ocean using the land-sea flag given in the L2 product (parameter **surf_type_01** – interpolated via nearest neighbor to 20Hz). (Since the initial focus is the Mediterranean basin, ice flags will be not considered). A basic threshold criteria on SLA and SWH is then used to reject aberrant measurements: Observations are rejected when absolute values of SLA > 2 m or SWH > 15 m. Finally, a specific analysis along each altimeter track allows us to reject invalid SLA measurements on ocean using locally defined thresholds.

This latter valid data selection is based on an iterative kσ editing applied on SLA and based on two main steps. The processing is applied on each track individually. At each step, the k coefficient is optimized in order to reach a pre-defined data rejection rate. This assures the detection of invalid measurement while maximizing the availability of valid measurements. During the first step, SLA data outliers are rejected considering a k1σ criteria, σ being the SLA variability along the track considered and k1 depending on the statistical ocean variability on the location considered. K1 has a minimal value (set to 5) and is linearly amplified with the ocean variability. This allows the editing to relax the threshold criteria in high variability areas and avoid a too severe data rejection (e.g. regions of intense mesoscale dynamics). In the second step, the track considered is iteratively processed in order to reject invalid SLA measurements using a k2σ criteria applied on the short wavelengths SLA signal dominated by measurement noise. The short wavelength content of the SLA is extracted using a Lanczos-2 filtering (cutoff frequency of roughly 43 km), σ is estimated at each iteration and k2 depends

on the SWH signal using the nearly linear relation observed between the short wavelength SLA content (dominated by measurement noise) and the SWH for SWH higher than ~2m. For lower SWH values, k2 is set to 3. This avoid a too severe rejection of the SLA measurements in high SWH areas, where the noise measurement is usually higher. As in the case of the HFA corrections, the SWH signal used in the analysis has been filtered using a Lanczos-2 filter (for consistency, same cutoff wavelength as for the HFA). Currently, the relations between the K1 coefficient and ocean variability and the K2 coefficient and SWH used in the CO TDP have been defined using CryoSat-2 observations in the North Atlantic oceans. Relations based on CryoSat-2 observations in the Mediterranean are under development and will be included in future versions of the CO TDP.

4.5 Filtering

The aim of filtering SLA and ADT is to remove the high frequency content (instrumental noise) from those measurements, taking into account the correlation length of the oceanic signal. Filtering is applied after the individual SAR and LRM granules are combined into a single track. While our analysis did not evidence any significant bias between SAR and LRM observations in the Mediterranean basin, applying the filter after stitching the individual granules has the benefit of further smoothing the transition between the two modes and reducing the presence of filtering boundary effects. The filtering processing is performed with several steps given below:

1. Filling of the data holes by linear interpolation.
2. Filtering of SLA measurements over a whole pass using a median filter.
3. Filtering of filtered SLA measurements over a whole pass using a Lanczos-2 low pass filter.

Currently, to be consistent with the iterative editing analysis, the cutoff length of the Lanczos filter is set to roughly 43 km (corresponding to a half-window width of 127 points).

4.6 Uncertainty

The uncertainty associated with each SLA and ADT observation will be evaluated empirically through a statistical analysis of the CO TDP. This will provide an estimate of the precision of the observations (i.e. the spread around the expected value). Assessing the accuracy of the observations (i.e. how far the expected value is from the real value) will require, instead, direct comparison with external datasets (e.g. in-situ observations).

The uncertainty of each observation is computed as the contribution of two independent terms:

1. Large-wavelength errors
2. Short-wavelength errors

The large-wavelength errors are mission specifics and computed by the DUACS production system. They result from the contribution of 3 independent components:

a. Residual errors after geophysical correction are removed (mainly DAC)

b. Ionospheric correction errors due to the GIM model approximations (no dual frequency)
c. Error due to the lack of mean along track profile (because of CryoSat-2 drifting orbit). These re usually smaller than the previous two

The large-wavelength errors vary only as a function of location. They are thus provided over a static geographical grid of 1° by 1°. The errors are interpolated from the grid to the alongtrack positions of each observation via nearest-neighbour. The large-wavelength errors used for the CO TDP are likely overestimated: usually initial esitmates of such errors are subsequently refined via Objective Interpolation with each specific satellite dataset. However, such analysis has not yet been preformed in the DUACS production system for the CryoSat-2 mission.

The short-wavelength errors are the errors associate with individual measurements. For the CO TDP have been directly computed from the TDP1. The two main assumptions for our analysis are that:

a. Such errors are related to two main factors: SWH and Distance from the Coast
b. Consecutive 20 Hz measurements observe roughly the same geophysical conditions

Based on such assumptions, we first computed the SLA difference between consecutive observations, and we then binned those differences as a function of SHW (every 10 cm) and distance from the coast (every 1 km). The SLA error within each bin can be thus computed as the standard deviation of the observed differences divided by $\sqrt{2}$ (i.e., assuming the errors associated with two consecutive measurements to be completely independent).

Such analysis allowed us to reconstruct look up tables of the SLA error as a function of SWH and distance from the coast. Two distinct LUTs were computed independently for SAR and LRM observations. The resulting short-wavelength errors increase with SWH and approaching the coast. Error estimates become quite noisy for large distances from the coast and high SWH, mostly due to a reduced number of observations within those bins. Thus, the final LUT used to estimate the CP TDP uncertainty were obtained using the bins with SWH < 7 m and distance from the coast < 200 km. To further reduce the noise in the error estimates, the LUT were also smoothed with a Gaussian filter with an anisotropic kernel of 11 by 5 bins (distance from the coast dimension larger than the SWH one).

The uncertainty associated with individual SLA observations is thus

$$\varepsilon_{SLA} = LWE(lon, lat) + SWE(SWH, Dist\_to\_coast)$$

Since the ADT is computed as SLA+MDT, the error associated with individual ADT observations will be

$$\varepsilon_{ADT} = \frac{\sqrt{{\varepsilon_{SLA}}^2 + {\varepsilon_{MDT}}^2}}{2}$$

With ε_{MDT} the error associated with the MDT, also provided by CMEMS for each MTD estimate. As for the LWE, MDT errors are interpolated from the CMEMS grid to the CryoSat-2 tracks via nearest-neighbour.

Finally, the errors associated with individual SLA and ADT observations can be used to compute the errors of the filtered SLA and ADT as

$$\bar{\varepsilon} = \frac{\sqrt{\sum(w_i\ \varepsilon_i)^2}}{\sum w_i}$$

With w_i the weights of the filter kernel (again, we assume the errors of each individual observation within the kernel to be completely independent from each other).

5 EXAMPLES

5.1 Uncorrected Sea Surface Height

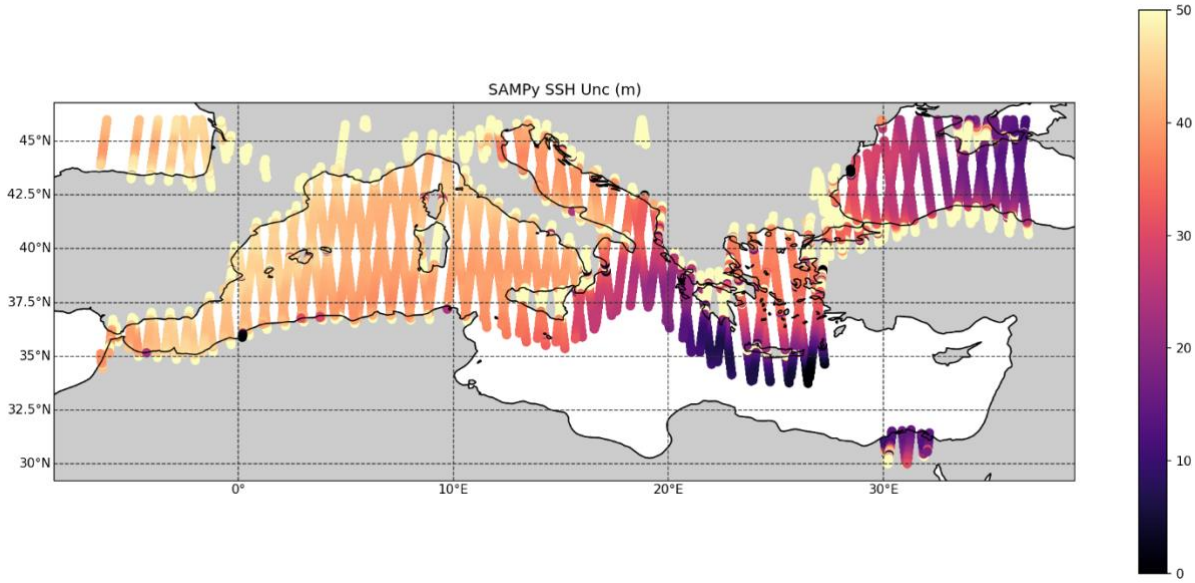

Figure 3. Example of uncorrected SSH obtained applying the Cryo-TEMPO implementation of the SAMOSA+ retracker on CryoSat-2 SAR observations track over the Mediterranean basin for cycle 63.

6 KNOWN ISSUES

The Cryo-TEMPO processing chain described in this ATBD has been implemented with the best standards available for ocean altimetry in order to achieve optimal performance in the coastal ocean. Nonetheless, there are still some known issues that remains unresolved in the current version of the

dataset which impact the quality of the derived geophysical variables. Further analysis is required to address these issues in future version of the Cryo-TEMPO CO TDP and further improve its overall quality. The most relevant ones include:

1. **Missing L1b variables for the SAMOSA+ retracker:**
   - The indexes of the zero-mask (i.e. gates in which to collocate the zeros in the SAMOSA DDM, as in Dinardo 2020, section 3.2.2 e)) are not reported in the PDGS COP L1b products. This forces users to apply an approximated zero-masking in the SAMOSA retracking which brings to errors in the estimation of the ocean geophysical parameters. It is recommended, as future evolution, to report the indexes of the zero-mask in the PDGS COP L1b products (as done in Sentinel-6 and soon also in Sentinel-3 STM PDGS).
   - Presently the thermal noise is estimated from the waveform early gates which is not an optimal option in the coastal zone or over polar oceans. It is, instead, recommended to provide in the PDGS COP L1b products the thermal noise estimated from the outer beams of the stack data as in Dinardo et al., 2018 (section 3.1.1).

2. **SARIn observations not included:** the CO TDP currently does not include **SARIn** observations. **SARIn** observations were acquired over the Mediterranean Sea only starting from December 2015, when the geographical mode mask was updated to include a **SARIn** mode area over the Aegean sea and to extend the **SARIn** mode area over the Alps to include the coastal area between Italy and France. These areas will be included in future version of the TDP, only after the SAMOSA+ retracker will be adapted and tested on **SARIn** data.

3. **New correction parameters:** As already mentioned in section 4, some of the new corrections applied in the Cryo-TEMPO CO processing chain make use of parametrizations and LUT which were not specifically derived for CryoSat-2 SAR observations over the Mediterranean Sea (e.g. LUT for the HFA were derived from global Saral/AltiKa SAR observations; parameters for the iterative editing were derived from CryoSat-2 SAR observations but over the North Atlantic; and LUT for the SSB correction were derived from global CryoSat-2 SAR observations but not using the SAMOSA+ retracker) . Cryo-TEMPO-specific parameters for those corrections will be implemented and included in future versions of the TDP.

7 REFERENCES

Abdalla S. (2012) Ku-Band Radar Altimeter Surface Wind Speed Algorithm, Marine Geodesy, 35:sup1, 276-298, DOI: 10.1080/01490419.2012.718676

Cancet, M., Lyard F., Toublanc F., Pineau-Guillou L., Sahuc E., Fouchet E., Dibarboure G., Picot N., The RegAt high-resolution regional tidal model in the North-East Atlantic Ocean: implementation and examples of applications, in preparation (2022)

CMEMS MEDITERRANEAN SEA MEAN DYNAMIC TOPOGRAPHY
SEALEVEL_MED_PHY_MDT_L4_STATIC_008_066
(https://catalogue.marine.copernicus.eu/documents/QUID/CMEMS-SL-QUID-008-063-066-067.pdf)

Desai, S., Wahr, J. & Beckley, B. Revisiting the pole tide for and from satellite altimetry. *J Geod* **89,** 1233–1243 (2015). https://doi.org/10.1007/s00190-015-0848-7

Dinardo S., Fenoglio, L., Buchhaupt C., Becker M., Scharroo R., Fernandes M. J, Benveniste, J. (2018). Coastal SAR and PLRM altimetry in German Bight and West Baltic Sea. Advances in Space Research. 62. http://doi.org/10.1016/j.asr.2017.12.018

Dinardo S. (2020): Techniques and applications for Satellite SAR Altimetry over water, land and ice. PhD Dissertation Thesis. 56, Darmstadt, Germany, Technische Universität, ISBN 978-3-935631-45-7. https://doi.org/10.25534/tuprints-00011343

Ducet, N., P.-Y. Le Traon, and G. Reverdin, 2000: Global high resolution mapping of ocean circulation from TOPEX/Poseidon and ERS-1 and -2. *J. Geophys. Res.*, **105,** 19477-19498.

Fenoglio-Marc L., Dinardo S., Scharroo R., Roland A., Dutour Sikiric M., Lucas B., Becker M., Benveniste J., Weiss R. (2015). The German Bight: A validation of CryoSat-2 altimeter data in SAR mode, Advances in Space Research, 55, 11, 2641-2656. http://dx.doi.org/10.1016/j.asr.2015.02.014

Khvorostovsky, K.; Hendricks, S.; Rinne, E. Surface Properties Linked to Retrieval Uncertainty of Satellite Sea-Ice Thickness with Upward-Looking Sonar Measurements. Remote Sens. 2020, 12, 3094. https://doi.org/10.3390/rs12183094

Kurtz N. T., Galin N., Studinger, M. (2014). An improved CryoSat-2 sea ice freeboard retrieval algorithm through the use of waveform fitting, Cryosphere, 8, 1217-1237.

Labroue, S., P. Gaspar, J. Dorandeu, O. Z. Zanifé, F. Mertz, P. Vincent, and D. Choquet, 2004: Nonparametric estimates of the sea state bias for the Jason-1 radar altimeter. *Mar. Geod.*, **27**, 453–481

Lievin, M., C. Kocha, B. Courcol, S. Philipps, I. Denis, T. Guinle, C. Nogueira Loddo, G. Dibarboure, N. Picot, F. Bignalet Cazalet, 2020: REPROCESSING of SEA LEVEL L2P products for 28 years of altimetry missions. OSTST 2020 virtual meeting.

https://meetings.aviso.altimetry.fr/fileadmin/user_upload/tx_ausyclsseminar/files/OSTST2020_Reprocessing_L2P_2020.pdf

Markus, T. and Cavalieri, D.J. (1998). Snow Depth Distribution Over Sea Ice in the Southern Ocean from Satellite Passive Microwave Data. In Antarctic Sea Ice: Physical Processes, Interactions and Variability, M.O. Jeffries (Ed.). https://doi.org/10.1029/AR074p0019

Paul, S., Hendricks, S., Ricker, R., Kern, S., and Rinne, E.: Empirical parametrization of Envisat freeboard retrieval of Arctic and Antarctic sea ice based on CryoSat-2: progress in the ESA Climate Change Initiative, The Cryosphere, 12, 2437–2460, https://doi.org/10.5194/tc-12-2437-2018, 2018.

Quartly, G.D., W.H.F. Smith and M. Passaro, (2019). Removing intra-1 Hz covariant error to improve altimetric profiles of <sigma>0 and sea surface height, IEEE Trans. Geosci. Rem. Sens., 57(6), 3741–3752, doi: 10.1109/iTGRS.2018.2886998

Ray C., Martin-Puig C., Clarizia M.P., Ruffini G., Dinardo S., Gommenginger C., Benveniste J. (2015). SAR Altimeter Backscattered Waveform Model, IEEE Trans. GeoSci. and Rem. Sens., 53, 2, 911 – 919. http://dx.doi.org/10.1109/TGRS.2014.2330423

Ricker, R., Hendricks, S., Helm, V., Skourup, H., and Davidson, M.: Sensitivity of CryoSat-2 Arctic sea-ice freeboard and thickness on radar-waveform interpretation, The Cryosphere, 8, 1607–1622, https://doi.org/10.5194/tc-8-1607-2014, 2014.

Rostosky, P., Spreen, G., Farrell, S. L., Frost, T., Heygster, G., & Melsheimer, C. (2018). Snow depth retrieval on Arctic sea ice from passive microwave radiometers—Improvements and extensions to multiyear ice using lower frequencies. Journal of Geophysical Research: Oceans, 123, 7120– 7138. https://doi.org/10.1029/2018JC014028

Taburet, G., Sanchez-Roman, A., Ballarotta, M., Pujol, M.-I., Legeais, J.-F., Fournier, F., Faugere, Y., and Dibarboure, G.: DUACS DT2018: 25 years of reprocessed sea level altimetry products, Ocean Sci., 15, 1207–1224, https://doi.org/10.5194/os-15-1207-2019, 2019

Tran N. (2018): “CS2 ESL tuning activities: wind speed and SSB”, Technical Report CLS-SPA-18-0007/CLS-COP-18-0001

Tran N ., D. Vandemark, E. D. Zaron, P. Thibaut, G. Dibarboure and N. Picot (2019): Assessing the effects of sea-state related errors on the precision of high-rate Jason-3 altimeter sea level data. Advance in Space Res., in press. https://doi.org/10.1016/j.asr.2019.11.034

Tseng K.H., Shum C.K., Yi Y., Fok H.S., Kuo C.Y., Lee H., Cheng X., Wang X. (2013). Envisat altimetry radar waveform retracking of quasi-specular echoes over the ice-covered Qinghai lake. Terr. Atmos. Ocean. Sci. ,24, 615–627. http://dx.doi.org/10.3319/TAO.2012.12.03.01

Warren, S. G., Rigor, I. G., Untersteiner, N., Radionov, V. F., Bryazgin, N. N., Aleksandrov, Y. I., & Colony, R. (1999). Snow Depth on Arctic Sea Ice, Journal of Climate, 12(6), 1814-1829. Retrieved Feb 17, 2021, from https://journals.ametsoc.org/view/journals/clim/12/6/1520-0442_1999_012_1814_sdoasi_2.0.co_2.xml